Theoretical analysis of electromagnetic exposure to wireless charging systems for deep-body implantable devices

Icaro Soares, Ronan Sauleau, Denys Nikolayev

STUDENT PAPER

Theoretical analysis of electromagnetic exposure to wireless charging systems for deep-body implantable devices

Icaro Soares (/user/9993) [1], Ronan Sauleau (/user/1246) [1] & Denys Nikolayev (/user/6735) [1]

[1] *IETR (Institut d'Électronique et des Technologies du numéRique) UMR–6164, Univ Rennes, CNRS, Rennes, France, 35700*

BioEM2021, Ghent, Belgium, Sep 26 - 30, 2021 *(/node/37973)*

Keywords: Dosimetry (computational), RF/Microwaves, Completed (unpublished)

Presented by: Icaro Soares

Wireless Power Transfer (WPT) techniques allow significant miniaturisation of implanted medical devices. However, the electromagnetic exposure of the body tissues must be accurately accessed to ensure safe operation. This study, therefore, analyses the exposure induced by the magnetic- and electric-type antenna transmitters over the frequency range of 100-MHz–5-GHz. The normalised power absorption, specific absorption rate (SAR) and WPT efficiency are analysed and presented. The results demonstrate the existence of an optimal operating frequency at which the maximum efficiency, minimum power absorption, and low SAR are simultaneously observed.

Introduction

Application of Wireless Power Transfer (WPT) techniques to miniature body-implanted devices allows the development of less invasive medical procedures and more reliable treatments [Nikolayev et al., 2019b; Poon, 2014]. As a particular example, significant miniaturisation of cardiac stimulators can be achieved through WPT once it eliminates the need for batteries—one of the most space-consuming components in these devices. It also minimises the frequency of surgical interventions required to replace the device once the batteries are empty. For this reason, different WPT techniques have been investigated and applied for pacemaker powering or wireless recharge. For instance, inductive WPT is usually employed to charge subcutaneous pacemakers due to its low implantation depth, and, in these cases, this approach achieves high efficiency [Liu et al., 2019; Campi et al., 2016b]. However, for deeply implanted stimulators, such as the miniature ones implanted inside the heart, midfield WPT can deliver higher power levels to the receiver when compared with other techniques [Ho et al., 2014; Asif et al., 2019; Shah et al., 2019].

However, to safely power these devices, the exposure to electromagnetic fields is a prime concern. Due to the highly dispersive, lossy, and heterogeneous characteristics of body tissues, the application of conventional WPT techniques can be underperforming or even hazardous [Campi et al., 2016a]. Consequently, the WPT system's parameters—the frequency, implantation depth, nature of the source—must be judiciously analysed to get an optimum trade-off between efficiency and exposure levels [Nikolayev et al., 2019c; Nikolayev et al., 2020]. This study, therefore, carries out a comparative study between an electric- and magnetic-type on-body equivalent sources that model a power

transmitter antenna for a deeply implanted pacemaker in the frequency range from 100 MHz to 5 GHz. For each source, the peak Specific Absorption Rate (SAR) [IEEE, 2019] is analysed along with the normalised power dissipation in the tissues and the WPT efficiency.

Methods

The problem is formulated through a 2D heterogeneous realistic model of the human pectoral region with nine dispersive tissues, as shown in Figure 1(a). The electromagnetic properties of each tissue are assigned according to [Gabriel et al., 1996] and their densities ρ according to the average values provided in [Mcintosh and Anderson, 2010]. The pacemaker is represented by a circular region with a diameter of 2 mm [Ho et al., 2014] implanted in the heart at a distance d ≈ 37 mm from the skin. The pacemaker receiver is assumed to be perfectly matched to the wave impedance of the myocardium. On the other side, the transmitter is analysed as two different cases. The first case is the Electric Source (ES) that is modelled as a surface current density J_s = [cos((πx)/L), 0, 0], in which L is the length of the source (Figure 1B). The second case is the Magnetic Source (MS) represented as unitary out-of-plane electric currents on the edge of the source with opposite phases (Figure 1C). In both cases, the transmitter is also perfectly matched to the skin, which can be physically realised using a matching layer with high permittivity [Nikolayev et al., 2019a].

The z-axis invariance is assumed (i.e., E(x, y, z) = E(x, y)exp(ik$_z$z), where k_z is the out-of-plane wave number) to reduce the model order to the 2D section of the human pectoral. This approach is justified since it leads to the scenario in which the source and receiver are perfectly aligned along z-axis and the optimal focusing in xy-plane is obtained. From the dosimetry perspective, it also ensures that the region of maximum exposure is incuded in the section of the source. For instance, it represents the area close to the wires of a loop antenna in the case of MS and the middle section of a dipole or patch antenna for the ES. Note that more complex field configurations and therefore SAR distributions may arise from the sources radiating higher order harmonics, but their use is limited for application in lossy tissues due to increased losess in near field [Skrivervik et al.,].

This model is implemented in COMSOL Multiphysics®, and, from the time-harmonic electric E and magnetic H field results, the transmitted, received, and dissipated power can be respectively calculated as follows:

$$P_t = \oint_{\Omega_s} \left(\frac{1}{2}\mathbf{E} \times \mathbf{H}^*\right) \cdot \mathrm{d}\mathbf{s}, \qquad \text{(Eq. 1)}$$

$$P_r = \oint_{\Omega_r} \left(\frac{1}{2}\mathbf{E} \times \mathbf{H}^*\right) \cdot \mathrm{d}\mathbf{s}, \qquad \text{(Eq. 2)}$$

$$P_d = \frac{1}{2}\int_{\Omega_p} \sigma \left|\mathbf{E}\right|^2 \mathrm{d}v. \qquad \text{(Eq. 3)}$$

where σ is the tissue electric conductivity, , and indicate that the integrals are evaluated over the source and receiver surfaces as well as the tissue volume, respectively. The amount of power absorbed in the body tissues is normalised by the transmitted power P_{abs} as:

$$P_{\mathrm{abs}} \equiv \frac{\Re(P_d)}{\Re(P_t)}. \qquad \text{(Eq. 4)}$$

Similarly, the WPT efficiency η is defined as the ratio between the received and transmitted powers:

$$\eta \equiv \frac{\Re(P_r)}{\Re(P_t)}. \qquad \text{(Eq. 5)}$$

Finally, the local SAR is given by:

$$\mathrm{SAR} \equiv \frac{\sigma \left|\mathbf{E}\right|^2}{\rho}. \qquad \text{(Eq. 6)}$$

Results and Discussion

The P_t-normalised results for the peak SAR, total absorbed power, and the WPT efficiency are shown in Figure 2. For frequencies below 1.82 GHz, a Magnetic Source (MS) leads to a lower peak SAR, except between 575.4 MHz and 1.41 GHz, in which the Electric Source (ES) exhibits reduced levels. However, at higher frequencies, the MS induces SAR almost twice as higher. Subsequently, the normalised absorbed power decreases with the frequency for the ES, whereas for the MS, it stays around 98% for the almost entire analysed band, decaying only above 3.89 GHz. It can also

be noticed that around 1.86 GHz, due to local resonances of the source and tissue media, the ES shows increased P_{abs}, also evidenced by a slight reduction in the WPT efficiency before reaching its maximum at 2.09 GHz. This optimum frequency agrees with previous studies on the theoretical limits for the maximum WPT efficiency, considering an on-body ES source and the implantation depth of 37 mm [Soares et al., 2021]. On the other side, for this application, the magnetic transmitter performance is sub-optimal, with its maximum efficiency about ten times lower than the electric one. It is explained by the fact that the MS leads to lower power absorption and achieves higher efficiency as an electrically small antenna, i.e., $L < \lambda/10$ [Nikolayev et al., 2019a; Nikolayev et al., 2020]. However, considering the wavelength in the skin, the size of the MS is larger than this limit for the entire analysed band, which explains the ES leading to lower absorption levels.

When the spatial behaviour of normalised SAR in Figure 3 is considered, the highest absorption occurs at the skin for both source types. The ES exhibits the SAR maximum at the centre of the source. Moreover, the previously observed SAR reduction around 891.2 MHz can also be evidenced in the surface plots. Conversely, the MS yields the maximum SAR around its edges, becoming more intense as the frequency increases due to the conductivity being proportional to the frequency [Gabriel et al., 1996]. This peak of MS is still localised in the skin, whereas the SAR for the ES also increases in fat and muscle tissues above 1.82 GHz. Finally, the SAR levels at the vital organs are insignificant compared to the skin layer for both sources in the considered frequency range.

Conclusions

This study analysed the power absorption in a realistic human pectoral model in order to evaluate the induced electromagnetic exposure by WPT to deep-implanted pacemakers. The results revealed that for the considered body model and implantation depth, an electric source leads to lower power absorption and, consequently, higher efficiency in the analysed frequency range. Although a magnetic source achieves lower absorption and SAR at low frequencies, once the source's size is in the order of the wavelength in the tissues, it is outperformed by the electric one. To sum up, for both sources, the absorption is mostly localised in the skin and is insignificant in vital organs. A transmitter compliance with the skin exposure, therefore, ensures a safe operation of the wirelessly powered pacemakers.

Acknowledgment

This study was supported by the French region of Brittany through the SAD "EM-NEURO" project.

References

Asif SM, Iftikhar A, Braaten BD, Ewert DL, Maile K. 2019. A wide-band tissue numerical model for deeply implantable antennas for RF-powered leadless pacemakers. IEEE Access. 7:31031–31042.

Campi T, Cruciani S, De Santis V, Feliziani M. 2016a. EMF safety and thermal aspects in a pacemaker equipped with a wireless power transfer system working at low frequency. IEEE Trans. Microw. Theory Techn. 64:375–382.

Campi T, Cruciani S, Palandrani F, De Santis V, Hirata A, Feliziani M. 2016b. Wireless power transfer charging system for AIMDs and pacemakers. IEEE Trans. Microw. Theory Techn. 64:633–642.

Gabriel S, Lau RW, Gabriel C. 1996. The dielectric properties of biological tissues: III. Parametric models for the dielectric spectrum of tissues. Phys. Med. Biol. 41:2271–2293.

Ho JS, Yeh AJ, Neofytou E, Kim S, Tanabe Y, Patlolla B, Beygui RE, Poon ASY. 2014. Wireless power transfer to deep-tissue microimplants. Proc. Natl. Acad. Sci. U.S.A 111:7974–7979.

IEEE. 2019. IEEE standard for safety levels with respect to human exposure to electric, magnetic, and electromagnetic fields, 0 Hz to 300 GHz. IEEE Std C95.1-2019 (Revision of IEEE Std C95.1-2005/ Incorporates IEEE Std C95.1-2019/Cor 1-2019):1–312.

Liu C, Jiang C, Song J, Chau KT. 2019. An effective sandwiched wireless power transfer system for charging implantable cardiac pacemaker. IEEE Trans. Ind. Electron. 66:4108–4117.

Mcintosh RL, Anderson V. 2010. A comprehensive tissue properties database provided for the thermal assessment of a human at rest. Biophys. Rev. Lett. 05:129–151.

Nikolayev D, Joseph W, Skrivervik A, Zhadobov M, Martens L, Sauleau R. 2019a. Dielectric-loaded conformal microstrip antennas for versatile in-body applications. IEEE Antennas Wirel. Propag. Lett. 18:2686–2690.

Nikolayev D, Joseph W, Zhadobov M, Sauleau R, Martens L. 2019b. Optimal radiation of body-implanted capsules. Phys. Rev. Lett. 122:108101.

Nikolayev D, Joseph W, Zhadobov M, Sauleau R, Martens L, Skrivervik A. 2019c. Exposure assessment of body-implanted capsules in the 100-MHz-5-GHz range. In: . Proc. BioEM 2019. Bioelectromagnetics Society (BEMS). p. 63–67.

Nikolayev D, Skrivervik A, Joseph W, Martens L, Sauleau R, Zhadobov M. 2020. Minimizing electromagnetic exposure for wireless mm-size neural implants. In: . Proc. BioEM 2020. p. 345–349.

Poon ASY. 2014. Miniaturized biomedical implantable devices. In: . Implantable Bioelectronics. John Wiley & Sons, Ltd. p. 45–64.

Shah IA, Zada M, Yoo H. 2019. Design and analysis of a compact-sized multiband spiral-shaped implantable antenna for scalp implantable and leadless pacemaker systems. IEEE Trans. Antennas Propag. 67:4230–4234.

Skrivervik AK, Bosiljevac M, Sipus Z. Fundamental limits for implanted antennas: Maximum power density reaching free space. IEEE Trans. Antennas Propag. 67:4978–4988.

Soares IV, Gao M, Skrivervik AK, Sipus Z, Zhadobov M, Sauleau R, Nikolayev D. 2021. Physical bounds on implant powering efficiency using body-conformal WPT systems. In: . Proc. IEEE Wireless Power Transfer Conf. (WPTC 2021). San Diego, USA.

Figures

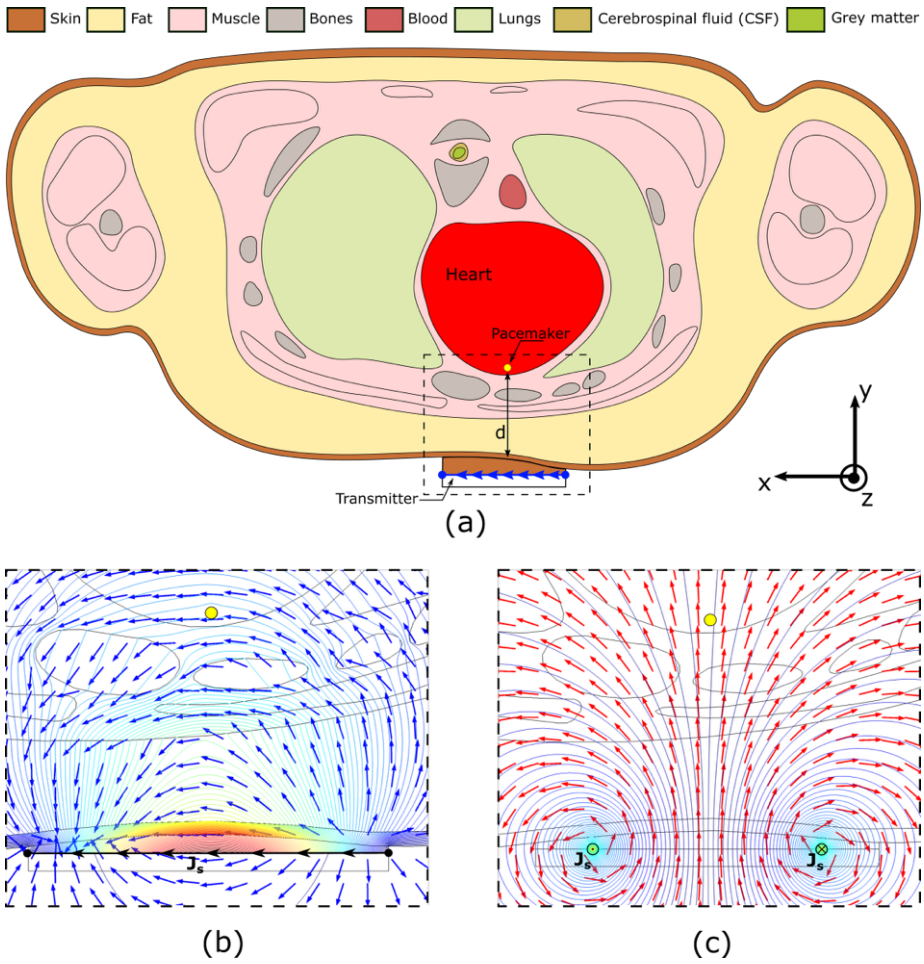

Figure 1. Problem formulation of WPT to a deep-tissue pacemaker: (a) Anatomical 2D model of a human pectoral region comprising nine dispersive tissues. An on-body source represents the transmitter, and the receiver is a pacemaker implanted inside the heart at a depth d. (b) Close-up view of the electric source modelled as a surface current density with the electric field distribution indicated by the blue arrows and the isolines for the magnetic field. (c) Close-up view of the magnetic source modelled as an out-of-plane current with the magnetic field distribution indicated by the red arrows and the isolines for the electric field.

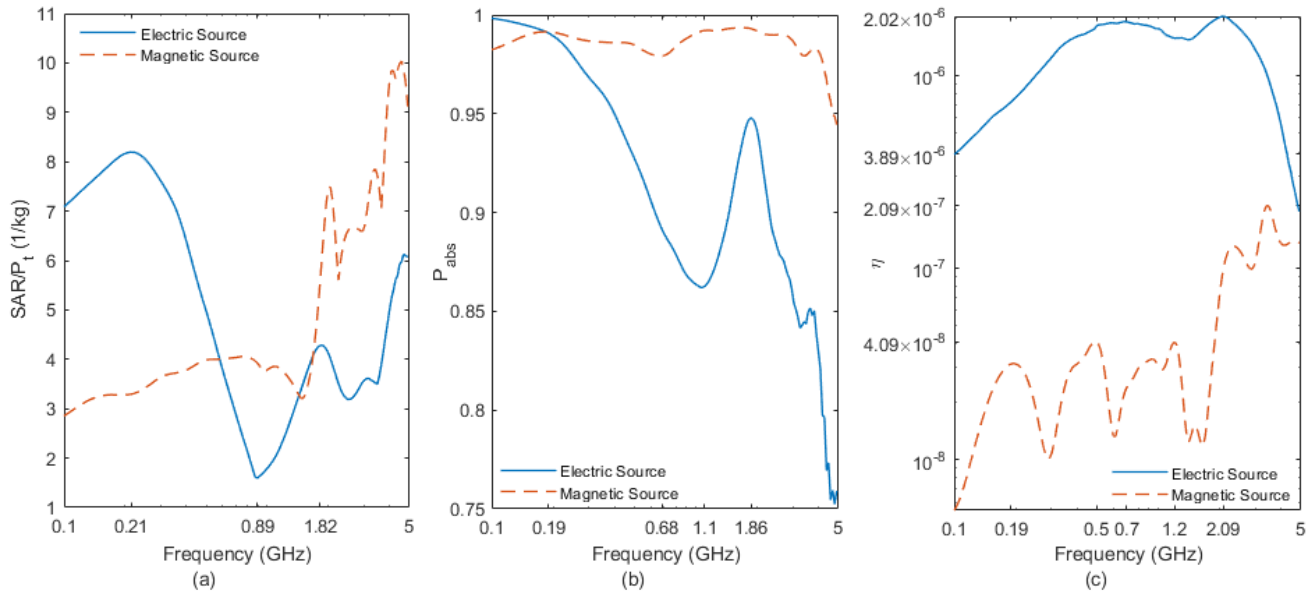

Figure 2. Results for (a) normalised peak SAR, (b) normalised absorbed power (P_{abs}) and (c) WPT efficiency (η) for the electric and magnetic sources.

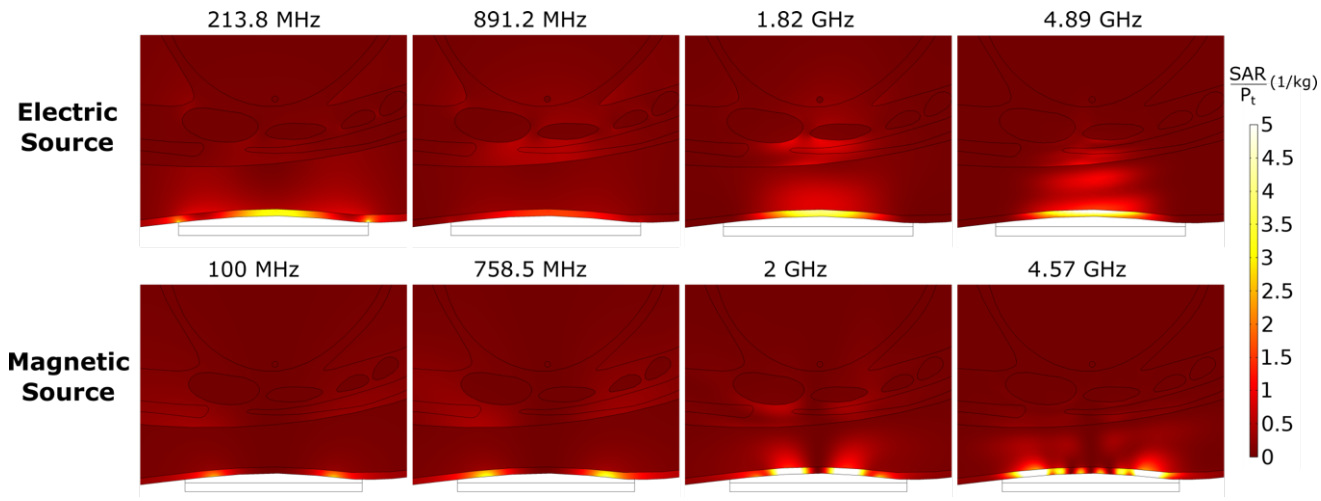

Figure 3. Colormaps for the peak SAR normalised by the transmitted power for the electric and magnetic sources.